

Available online at [www.sciencedirect.com](http://www.sciencedirect.com)

ScienceDirect

journal homepage: [www.elsevier.com/locate/watres](http://www.elsevier.com/locate/watres)

# Relating rejection of trace organic contaminants to membrane properties in forward osmosis: Measurements, modelling and implications

Ming Xie<sup>a</sup>, Long D. Nghiem<sup>a,\*</sup>, William E. Price<sup>b</sup>, Menachem Elimelech<sup>c</sup>

<sup>a</sup> Strategic Water Infrastructure Laboratory, School of Civil, Mining and Environmental Engineering, University of Wollongong, Wollongong, NSW 2522, Australia

<sup>b</sup> Strategic Water Infrastructure Laboratory, School of Chemistry, University of Wollongong, Wollongong, NSW 2522, Australia

<sup>c</sup> Department of Chemical and Environmental Engineering, Yale University, New Haven, CT 06520-8286, USA

## ARTICLE INFO

### Article history:

Received 19 August 2013

Received in revised form

17 November 2013

Accepted 19 November 2013

Available online 1 December 2013

### Keywords:

Forward osmosis

Solute rejection

Membrane surface charge

Trace organic contaminants (TrOCs)

Permeate flux

Pore hindrance transport model

Pore size

## ABSTRACT

This study elucidates the relationship between membrane properties and the rejection of trace organic contaminants (TrOCs) in forward osmosis (FO). An asymmetric cellulose triacetate (CTA) and a thin-film composite (TFC) polyamide FO membrane were used for this investigation. The effective average pore radius ( $r_p$ ), selective barrier thickness over porosity parameter ( $l/\epsilon$ ), surface charge, support layer structural parameter ( $S$ ), pure water permeability coefficient ( $A$ ) and salt (NaCl) permeability coefficient ( $B$ ) of the two membranes were systematically characterised. Results show that measured rejection of TrOCs as a function of permeate water flux can be well described by the pore hindrance transport model. This observation represents the first successful application of this model, which was developed for pressure-driven nanofiltration, to an osmotically-driven membrane process. The rejection of charged TrOCs by the CTA and TFC membranes was high and was governed by both electrostatic repulsion and steric hindrance. The TFC membrane exhibited higher rejection of neutral TrOCs with low molecular weight than the CTA membrane, although the estimated pore size of the TFC membrane (0.42 nm) was slightly larger than that of the CTA membrane (0.37 nm). This higher rejection of neutral TrOCs by the TFC membrane is likely attributed to its active layer properties, namely a more effective active layer structure, as indicated by a larger  $l/\epsilon$  parameter, and pore hydration induced by the negative surface charge.

Crown Copyright © 2013 Published by Elsevier Ltd. All rights reserved.

## 1. Introduction

More than four billion people live in areas where drinking water security and ecosystem biodiversity are being threatened by freshwater shortages. This problem is being

exacerbated by urbanization, population growth and climate change (Grant et al., 2012). As a result, significant research efforts have been made to facilitate the extraction of clean water from unconventional resources, such as seawater and wastewater effluent, to augment drinking water supplies. Membrane filtration processes, such as reverse osmosis (RO)

\* Corresponding author. Tel.: +61 2 4221 4590.

E-mail address: [longn@uow.edu.au](mailto:longn@uow.edu.au) (L.D. Nghiem).

0043-1354/\$ – see front matter Crown Copyright © 2013 Published by Elsevier Ltd. All rights reserved.

<http://dx.doi.org/10.1016/j.watres.2013.11.031>

and nanofiltration (NF), have contributed to a remarkable increase in the utilisation of unconventional water resources (Elimelech and Phillip, 2011; Shannon et al., 2008). However, numerous trace organic contaminants (TrOCs) are being frequently detected in wastewater and sewage-impacted water bodies (Basile et al., 2011; Carballa et al., 2004; Schwarzenbach et al., 2006; Snyder et al., 2003). As a result, in addition to existing membrane processes such as NF and RO, novel treatment technologies, which can potentially provide a more efficient and cost-effective barrier against TrOCs, have also been explored.

Forward osmosis (FO) is one such novel membrane process that has the potential to advance water and wastewater treatment (Cath et al., 2006; Zhao et al., 2012). In FO, a semi-permeable membrane is placed between a feed solution and a concentrated draw solution with high osmotic pressure. The extraction of water is driven by the osmotic pressure difference and, at the same time, salt and contaminants in the feed solution are being rejected by the FO membrane. To produce freshwater, FO is usually combined with pressure-driven membrane processes, such as NF and RO (Hoover et al., 2011; Shaffer et al., 2012; Yangali-Quintanilla et al., 2011), or thermal processes, such as conventional column distillation (McCutcheon et al., 2005; McGinnis and Elimelech, 2007) and membrane distillation (Cath et al., 2005; Martinetti et al., 2009). In these hybrid treatment systems, TrOCs in the feed are first subjected to rejection by the FO membrane and then by the subsequent process that is used to both concentrate the draw solution and produce freshwater, thereby providing a dual barrier for TrOCs. Hence, it is of paramount importance to better elucidate the removal of TrOCs in the FO process.

High removal efficiency of TrOCs by the FO process has been demonstrated in several previous studies. Cartinella et al. (2006) found a near complete rejection of three hormones in FO. Cath et al. (2010) reported the rejection of six TrOCs, ranging from 72% (salicylic acid) to more than 99% (diclofenac). A comprehensive study on the removal of 23 TrOCs revealed that the rejection of charged TrOCs was consistently above 80%, whereas the rejection of neutral TrOCs varied from 40 to 90% (Hancock et al., 2011b). A similar observation was also reported by Valladares Linares et al. (2011) when examining the removal of 13 TrOCs. Alturki et al. (2013) elucidated the mechanisms governing the rejection of 40 TrOCs compounds by FO, indicating that the rejection of charged TrOCs is governed by both electrostatic interaction and size exclusion, while rejection of neutral compounds is dominated by size exclusion.

It is noteworthy that to date most studies investigating the removal of TrOCs by the FO process employed an asymmetric cellulose triacetate (CTA) membrane. Given the recent progress in the development of new membrane materials for FO applications, polyamide thin-film composite (TFC) membranes have been recently introduced. These TFC membranes have been reported to have higher water permeability and solute rejection compared to their CTA counterparts (Wang et al., 2010; Wei et al., 2011; Yip et al., 2010). Because there are considerable differences between asymmetric CTA and polyamide TFC membranes, it is worthwhile to systematically examine their rejection performance and provide insights into

the relationship between membrane properties and TrOCs rejection.

In this study, we examine and compare the rejection of 12 TrOCs by an asymmetric CTA and a polyamide TFC membrane as a function of permeate water flux. Key properties of the CTA and TFC membranes were characterised to facilitate the understanding of their TrOC rejection behaviour. The membrane pore hindrance transport model was used to predict the rejection of the TrOCs as a function of permeate water flux and model predictions were compared with the experimentally measured data. Rejection of TrOCs by the CTA and TFC membranes was related to the membrane properties and mechanisms responsible for the rejection of TrOCs were proposed and elucidated.

## 2. Materials and methods

### 2.1. Trace organic contaminants

Twelve TrOCs, frequently detected in secondary treated effluent and sewage-impacted water bodies at trace levels, were used for this investigation. The TrOCs were selected to cover a diverse range of properties including charge, hydrophobicity and molecular weight (Table 1). A combined stock solution containing 1 g/L of each TrOC was prepared in methanol. The stock solution was kept at  $-18^{\circ}\text{C}$  in the dark and was used within one month.

### 2.2. Forward osmosis and reverse osmosis systems

A bench-scale FO system consisting of a cross-flow membrane cell with a total effective membrane area of  $123.5\text{ cm}^2$  was employed. The membrane cell had two identical and symmetrical flow chambers with length, width and channel height of 130, 95, and 2 mm, respectively. The circulation flow rates of the feed and draw solutions were kept constant at 1 L/min (corresponding to a cross-flow velocity of 9 cm/s). The draw solution reservoir was placed on a digital balance (Mettler Toledo Inc., Hightstown, NJ) and weight changes were recorded by a computer to calculate the permeate water flux. A conductivity controller (Cole–Parmer, Vernon Hills, IL) was used to maintain a constant draw solution concentration when inorganic salt was used as the draw solute. Further details of this conductivity control system are available elsewhere (Xie et al., 2012a).

A bench-scale RO system with a rectangular stainless-steel cross-flow cell was used to characterise the membrane pore radius and membrane transport parameters. The RO membrane cell had an effective membrane area of  $40\text{ cm}^2$ , with channel length, width and depth of 100, 40 and 2 mm, respectively. The unit was equipped with a Hydra-Cell pump (Wanner Engineering Inc., Minneapolis, MN). The temperature of the feed solution was kept constant using a chiller/heater (Neslab RTE 7). Permeate flow was measured by a digital flow meter (FlowCal 5000, Tovatech, South Orange, NJ).

### 2.3. Characterization of forward osmosis membranes

An asymmetric CTA and a polyamide TFC membrane were acquired from Hydration Technology Innovations (Albany,

**Table 1 – Key physicochemical properties of selected trace organic contaminants.**

| Compound          | Charge<br>(at pH 6.5) | Molecular weight<br>(g/mol) | Log D <sup>a</sup><br>(at pH 6.5) | pK <sub>a</sub> <sup>a</sup> | Diffusion<br>coefficient <sup>b</sup><br>(× 10 <sup>−10</sup> m <sup>2</sup> /s) | Stokes<br>radius <sup>c</sup> (nm) |
|-------------------|-----------------------|-----------------------------|-----------------------------------|------------------------------|----------------------------------------------------------------------------------|------------------------------------|
| Sulfamethoxazole  | Negative              | 253                         | −0.96                             | 5.18                         | 5.61                                                                             | 0.38                               |
| Diclofenac        |                       | 296                         | 1.77                              | 4.18                         | 5.16                                                                             | 0.41                               |
| Bezafibrate       |                       | 362                         | −0.93                             | 3.29                         | 4.64                                                                             | 0.46                               |
| Amitriptyline     | Positive              | 277                         | 2.28                              | 9.18                         | 5.35                                                                             | 0.40                               |
| Trimethoprim      |                       | 290                         | 0.27                              | 7.04                         | 5.22                                                                             | 0.41                               |
| Caffeine          | Neutral               | 194                         | −0.63                             | 0.52                         | 6.46                                                                             | 0.33                               |
| Atrazine          |                       | 216                         | 2.64                              | 2.27                         | 6.10                                                                             | 0.35                               |
| Primidone         |                       | 218                         | 0.83                              | 12.26                        | 6.07                                                                             | 0.35                               |
| Carbamazepine     |                       | 236                         | 1.89                              | 13.94                        | 5.82                                                                             | 0.36                               |
| Linuron           |                       | 249                         | 3.12                              | 12.13                        | 5.66                                                                             | 0.37                               |
| Pentachlorophenol |                       | 266                         | 2.95                              | 4.68                         | 5.46                                                                             | 0.39                               |
| Triclosan         |                       | 290                         | 5.28                              | 7.8                          | 5.22                                                                             | 0.41                               |

<sup>a</sup> Values for pK<sub>a</sub> and log D were obtained from the SciFinder Scholar (ACS) database.  
<sup>b</sup> Calculated using the Wilke and Chang equation (Wilke and Chang, 1955) at 25 °C.  
<sup>c</sup> Calculated using Stokes–Einstein equation.

OR) and Oasys Water (Boston, MA), respectively. The CTA membrane is composed of a cellulose triacetate layer with an embedded woven support mesh (Cath et al., 2006; McCutcheon and Elimelech, 2008). The TFC membrane is made of a thin selective polyamide active layer on top of a porous polysulfone support layer (Cath et al., 2013; McGinnis et al., 2013).

### 2.3.1. Membrane transport parameters

Key membrane transport parameters were characterised following the protocol previously described by Cath et al. (2013), including pure water permeability coefficient of the active layer,  $A$ , the salt (NaCl) permeability coefficient of the active layer,  $B$ , and the structural parameter of the support layer,  $S$ . Briefly, the membrane  $A$  and  $B$  values were determined using the RO cross-flow filtration system (Section 2.2). The membrane  $A$  value was measured at a pressure of 10 bar using deionised water. NaCl was then added to the feed solution to determine the  $B$  value. The RO system was stabilised for 2 h before recording permeate water flux with 2000 mg/L NaCl solution,  $J_w^{\text{NaCl}}$ , and taking feed and permeate samples to determine the observed NaCl rejection,  $R_o$ . Membrane  $A$  value was calculated by dividing the pure water permeate flux ( $J_w^{\text{RO}}$ ) by the applied hydraulic pressure,  $\Delta P$ :

$$A = J_w^{\text{RO}} / \Delta P \quad (1)$$

The observed salt (NaCl) rejection,  $R_o$ , was calculated from the difference between the bulk feed ( $c_b$ ) and permeate ( $c_p$ ) salt concentrations,  $R_o = 1 - c_p/c_b$ , and then the membrane  $B$  value was determined from:

$$B = J_w^{\text{NaCl}} \left( \frac{1 - R_o}{R_o} \right) \exp \left( - \frac{J_w^{\text{NaCl}}}{k_f} \right) \quad (2)$$

where  $k_f$  is the mass transfer coefficient for the cross-flow of RO membrane cell.

The mass transfer coefficient ( $k_f$ ) was experimentally determined using the Sutzkover et al. method (Sutzkover et al., 2000). Using the permeate and feed salt concentrations (and thus, the corresponding osmotic pressures based on

van't Hoff equation,  $\pi_p$  and  $\pi_b$ , respectively), the applied pressure ( $\Delta P$ ), the pure water flux ( $J_w^{\text{RO}}$ ), and the permeate flux with the 2000 mg/L NaCl solution ( $J_w^{\text{NaCl}}$ ) enabled the evaluation of the salt concentration at the membrane surface. This membrane surface concentration was used with thin-film theory for concentration polarization to determine  $k_f$ :

$$k_f = \frac{J_w^{\text{NaCl}}}{\ln \left[ \frac{\Delta P}{\pi_b - \pi_p} \left( 1 - \frac{J_w^{\text{NaCl}}}{J_w^{\text{RO}}} \right) \right]} \quad (3)$$

The membrane structural parameter,  $S$ , was evaluated in the cross-flow FO setup (Section 2.2). The water flux  $J_w^{\text{FO}}$ , using a 0.5 M NaCl draw solution and deionised water feed solution was measured with the membrane in FO mode (i.e., active layer facing the feed solution). The membrane  $S$  value was determined using:

$$S = \frac{D_s}{J_w^{\text{FO}}} \ln \left( \frac{B + A\pi_{D,b}}{B + J_w + A\pi_{F,m}} \right) \quad (4)$$

where  $D_s$  is the bulk solution diffusivity of the draw solute,  $\pi_{D,b}$  is the bulk osmotic pressure of the draw solution, and  $\pi_{F,m}$  is the osmotic pressure at the membrane surface on the feed side (zero for deionised water feed). The values of  $A$  and  $B$  in Eq. (4) were calculated using Eqs. (1) and (2).

### 2.3.2. Membrane average pore radius

Erythritol, xylose, and glucose (Sigma–Aldrich, Saint Louis, MO) were used as the reference organic solutes to estimate the membrane active layer effective pore size. The solutes were individually dissolved in Milli-Q water to obtain a concentration of 40 mg/L (as total organic carbon (TOC)). Prior to the RO filtration experiments with these reference organic solutes, the membrane was pre-compacted at 18 bar for 1 h and subsequent experiments were conducted at 8, 10, 12, 14, and 16 bar with a cross-flow velocity of 25 cm/s. At each pressure value, the RO filtration system was operated for 1 h before taking permeate and feed samples for analysis.

The membrane average pore radius was determined based on the pore hindrance transport model previously described by Nghiem et al. (2004) for nanofiltration. In this model, the FO

membrane was considered as a bundle of cylindrical capillary tubes with the same radius. In addition, we assumed that the spherical solute particles enter the membrane pores in random fashion. It is noteworthy that the pore hindrance model was developed for neutral and non-adsorptive solutes. Thus, it may underestimate the rejection of charged organic compounds and overestimate the rejection of hydrophobic organic compounds.

In the pore hindrance transport model, the ratio of solute radius ( $r_s$ ) to the membrane pore radius ( $r_p$ ),  $\lambda = r_s/r_p$ , is related by the distribution coefficient  $\phi$  when only steric interactions are considered:

$$\phi = (1 - \lambda)^2 \quad (5)$$

The real rejection of the reference organic solutes ( $R_r$ ) was determined from:

$$R_r = 1 - \frac{c_l}{c_o} = 1 - \frac{\phi K_c}{1 - \exp(-P_e)(1 - \phi K_c)} \quad (6)$$

where  $c_o$  and  $c_l$  are the solute concentration just outside the pore entrance and pore exit, respectively;  $\phi$  is the distribution coefficient for hard-sphere particles when only steric interactions are considered;  $K_c$  is the hydrodynamic hindrance coefficient for convection; and  $P_e$  is the membrane Peclet number defined as:

$$Pe = \frac{K_d J_v l}{K_d D \varepsilon} \quad (7)$$

Here,  $K_d$  is the hydrodynamic hindrance coefficient for diffusion,  $J_v$  is the membrane volumetric permeate flux,  $D$  is the Stokes–Einstein diffusion coefficient,  $l$  is the theoretical pore length (i.e., active layer thickness), and  $\varepsilon$  is the effective porosity of the membrane active later. Details on the calculations of  $P_e$ ,  $K_c$  and  $K_d$  are given elsewhere (Bungay and Brenner, 1973; Nghiem et al., 2004). The  $\phi K_c$  and  $\phi K_d$  are two hindrance factors accounting for solute convection and diffusion, respectively. These factors are significantly dependent on  $\lambda$ , the ratio of solute radius ( $r_s$ ) to the membrane pore radius ( $r_p$ ).

The real rejection in Eq. (6) is linked to the observed rejection  $R_o$  using the film theory which accounts for concentration polarization:

$$\ln \left( \frac{1 - R_r}{R_r} \right) = \ln \left( \frac{1 - R_o}{R_o} \right) - \frac{J_v}{k_f} \quad (8)$$

where  $k_f$  is the mass transfer coefficient and  $J_v$  is the water permeate flux.

### 2.3.3. Membrane surface charge

The zeta potential of the membrane surface was determined using a SurPASS electrokinetic analyser (Anton Paar GmbH, Graz, Austria). The value for each surface was calculated from the measured streaming potential using the Fairbrother–Mastin approach (Elimelech et al., 1994). All streaming potential measurements were conducted in a background electrolyte solution containing 10 mM KCl. The same electrolyte solution was used to flush the cell thoroughly prior to pH titration using either hydrochloric acid (1 M) or potassium hydroxide (1 M). All measurements were performed at room temperature (approximately 22 °C).

### 2.4. Trace organic contaminant rejection experiment

The TrOC stock solution was added to a background electrolyte solution (20 mM NaCl and 1 mM NaHCO<sub>3</sub>) to obtain a feed solution concentration of 2 µg/L. Either HCl (1 M) or NaOH (1 M) was used to adjust the initial pH value of the feed solution.

In FO experiments, the initial volumes of the feed and draw solutions were 4 and 1 L, respectively. The feed and draw solutions were kept at 25 ± 0.1 °C using a temperature controller (Neslab RTE 7). A new FO membrane sample was used for each experiment, which was concluded when 1 L water had permeated through the FO membrane (i.e., 25% water recovery). The reverse solute flux of NaCl was determined using electric conductivity measurements and an NaCl calibration curve. A 500 mL aliquot of sample from the feed and draw solutions were taken at the beginning and after 1 L water had permeated through the FO membrane for solid phase extraction (SPE) using Oasis HBL SPE cartridge and subsequent liquid chromatography-mass spectrometry (LC–MS) analysis.

### 2.5. Analysis of trace organic contaminants

The TrOC concentrations in the feed and draw solution samples were determined by liquid chromatography – mass spectrometry (LC–MS) using an electrospray ionization interface. The analysis was conducted in selective ion monitoring mode using a Shimadzu LC–MS 2020. Further details on the TrOC analytical method can be found in a previous publication (Xie et al., 2013).

## 3. Results and discussion

### 3.1. Membrane properties

#### 3.1.1. Transport parameters

Transport parameters of the CTA and TFC membranes are summarized in Table 2. The CTA membrane was found to have a lower pure water permeability coefficient ( $A$  value) and a higher structural parameter ( $S$  value) than the TFC membrane. As a result, using a 0.5 M NaCl draw solution and deionised water feed, the obtained average water fluxes of the CTA and TFC membranes were 5.4 and 15.1 L/m<sup>2</sup>h, respectively. Furthermore, the salt (NaCl) permeability coefficient of the CTA membrane was significantly higher than that of the TFC membrane (Table 2). Consequently, the reverse NaCl flux of the CTA membrane (82.7 mmol/m<sup>2</sup>h) was one order of

**Table 2 – Pure water permeability coefficient, salt (NaCl) permeability coefficient and membrane structural parameter (average ± standard deviation from duplicate experiments).**

| Membrane                                                          | CTA         | TFC         |
|-------------------------------------------------------------------|-------------|-------------|
| Pure water permeability coefficient, $A$ (L/m <sup>2</sup> h-bar) | 0.65 ± 0.03 | 4.70 ± 0.16 |
| Salt (NaCl) permeability coefficient, $B$ (L/m <sup>2</sup> h)    | 0.25 ± 0.07 | 0.16 ± 0.03 |
| Membrane structural parameter, $S$ (mm)                           | 0.67 ± 0.13 | 0.52 ± 0.11 |



magnitude higher than that for the TFC membrane (5.5 mmol/m<sup>2</sup>h) under the same operating conditions.

### 3.1.2. Surface charge

Zeta potential measurements suggested that the surface of the TFC membrane was significantly more negatively charged than that of the CTA membrane at an experimental pH of 6.5 (Fig. 1). The highly negatively charged surface of the TFC membrane can be attributed to the dissociation of free or uncross-linked carboxylic functional groups of the polyamide active skin layer (Petersen, 1993). On the other hand, the predominant functional group on the CTA membrane surface is hydroxyl (Mi and Elimelech, 2010), which can only be deprotonated at high pH. Tiraferri and Elimelech (2012) measured the distribution of negatively charged functional groups of the CTA membrane using the toluidine blue O method and reported that the number of negatively charged functional groups was negligible. Indeed, the marginal negative charge of the CTA membrane observed in Fig. 1 can be attributed to preferential adsorption of anions, such as chloride and hydroxide, onto the membrane surface (Childress and Elimelech, 1996; Elimelech and O'Melia, 1990).

### 3.1.3. Average pore radius and active layer structure

Real rejection ( $R_r$ ) of each reference organic solute was determined from observed rejection ( $R_o$ ) by accounting for concentration polarization effects using Eq. (7) and the mass transfer coefficient calculated from Eq. (3). The real rejections obtained at different permeate fluxes were used to calculate the membrane average membrane pore size based on the membrane pore hindrance transport model presented earlier (Eq. (6)). The parameters  $\phi K_c$  and  $P_e/J_v$  are uniquely related to  $R_r$ . Thus, they could be determined by fitting the reference organic solute rejection data to the model (Eq. (6)) using an optimization procedure (Solver, Microsoft Excel). Because the parameters  $\phi K_c$  and  $P_e/J_v$  can be expressed as a sole function of

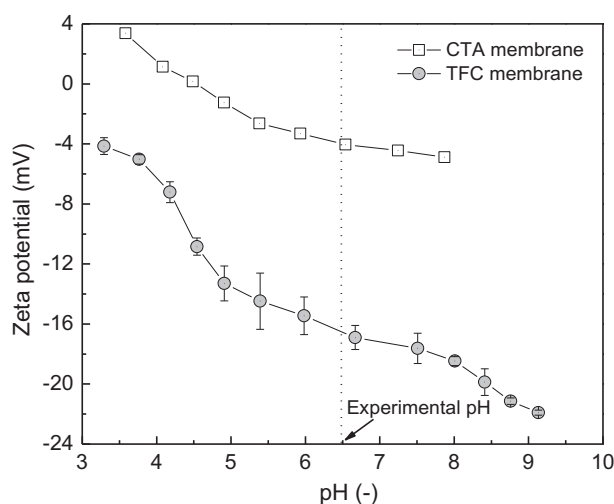


**Fig. 1** – Zeta potential of the CTA and TFC membranes as a function of solution pH. Measurements were carried out at 22 °C and a background electrolyte solution containing 10 mM KCl. Error bars represent a standard deviation from four replicate measurements using two membrane samples.

**Table 3** – Calculated average membrane pore radii ( $r_p$ ) and structural factors ( $l/\epsilon$ ) values of the CTA and TFC membrane active layers.

| Reference organic solute | Solute size $r_s$ (nm) | $\lambda = r_s/r_p$ | Pore radius $r_p$ (nm) | $l/\epsilon$ ( $\mu\text{m}$ ) |
|--------------------------|------------------------|---------------------|------------------------|--------------------------------|
| CTA membrane             |                        |                     |                        |                                |
| Erythritol               | 0.26                   | 0.79                | 0.33                   | 0.08                           |
| Xylose                   | 0.29                   | 0.76                | 0.38                   | 0.21                           |
| Glucose                  | 0.32                   | 0.80                | 0.40                   | 0.07                           |
| Average                  |                        |                     | 0.37                   | 0.11                           |
| TFC membrane             |                        |                     |                        |                                |
| Erythritol               | 0.26                   | 0.63                | 0.41                   | 3.48                           |
| Xylose                   | 0.29                   | 0.69                | 0.42                   | 1.84                           |
| Glucose                  | 0.32                   | 0.75                | 0.43                   | 1.03                           |
| Average                  |                        |                     | 0.42                   | 2.12                           |

**Table 4** – Reverse solute fluxes of the CTA and TFC membranes using different draw solutions.

| Draw solution           | Reverse draw solute flux (mmol/m <sup>2</sup> h) |              |
|-------------------------|--------------------------------------------------|--------------|
|                         | TFC membrane                                     | CTA membrane |
| 0.5 M NaCl              | 5.5                                              | 82.7         |
| 2.5 M MgSO <sub>4</sub> | 2.9                                              | 0.75         |
| 3 M glucose             | 1.5                                              | 0.67         |

the variable  $\lambda$  (which is the ratio of solute radius ( $r_s$ ) to membrane pore radius ( $r_p$ )),  $\lambda$  can be obtained for each reference organic solute and the membrane. The membrane average pore radius was then calculated for each reference solute

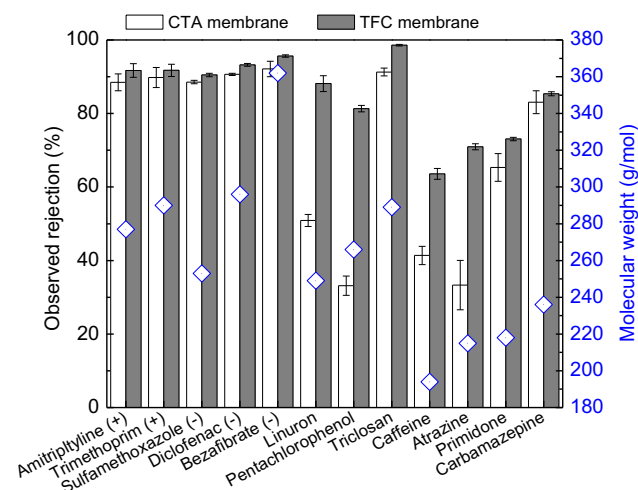


**Fig. 2** – Rejection of 12 TrOCs by the CTA and TFC membranes in FO. The molecular weight of each TrOC is indicated by the open diamond symbols. Experimental conditions: feed solution contained 2  $\mu\text{g/L}$  of each 12 TrOC in a background electrolyte (1 mM NaHCO<sub>3</sub> and 20 mM NaCl), and draw solutions for the CTA and TFC membranes were 0.5 M and 0.15 M NaCl, respectively, in order to generate the same water flux of 6 L/m<sup>2</sup>h. Temperatures of feed and draw solutions were 25  $\pm$  0.1 °C. Cross-flow rates of feed and draw solutions were 1 L/min (corresponding to cross-flow velocity of 9 cm/s). Error bars represent the standard deviation from four replicate measurements from two duplicate experiments.

rejection data. The membrane active layer structure indicated by the  $l/\epsilon$  value could also be determined from the values of  $\phi K_c$ ,  $P_e/J_v$ , and the diffusion coefficient of the reference organic solute. The obtained average pore radii and the  $l/\epsilon$  values of each membrane are shown in Table 3.

For each membrane, the pore radii obtained from the three reference organic solutes only slightly deviate from one to another. Results reported in Table 3 show that the average pore radius of the CTA membrane is smaller than that of the TFC membrane. In general agreement with their comparative average pore size, the CTA membrane had a smaller water permeability coefficient (Table 2) and a lower reverse draw solute flux (Table 4) in comparison to the TFC membrane when  $\text{MgSO}_4$  or glucose was used as draw solute. On the other hand, the active layer structural characteristic value,  $l/\epsilon$ , of the TFC membrane was one order of magnitude higher than that of the CTA membrane (Table 3). This significant difference in the active layer structure could result in a higher hindrance to solute transport by the TFC membrane compared to the CTA membrane (Nghiem et al., 2004; Schäfer et al., 2011). In addition, the TFC membrane pores are hydrated due to the existence of charged functional groups within its polyamide active layer (Raghunathan and Aluru, 2006). Such adsorption of water molecules within the membrane pore (i.e., the hydration of the membrane pore) could narrow the effective membrane pore

size, thereby enhancing the solute hindrance. As a result, both the active layer structure and pore hydration likely play an important role in feed solute transport through the membrane. Indeed, the TFC membrane active layer with higher solute hindrance and narrowed membrane pore exhibited better separation performance (i.e., lower B value and reverse NaCl flux) compared with the CTA membrane. This hypothesis will be further examined by comparing the rejection of TrOCs by the CTA and TFC membranes in the following section.

### 3.2. Rejection of trace organic contaminants

#### 3.2.1. General behaviour

Observed rejections of charged and neutral TrOCs by either the CTA or TFC membranes were markedly different for FO experiments at the same permeate water flux of 6 L/m<sup>2</sup>h (or 1.68  $\mu\text{m/s}$ ) (Fig. 2). Although the chemistry and intrinsic properties of the CTA and TFC membranes are different, rejection of charged TrOCs by both membranes were generally higher than those of neutral TrOCs, which is consistent with previous studies (Alturki et al., 2013; Valladares Linares et al., 2011; Xie et al., 2012b). These charged TrOCs may be rejected by both size exclusion and electrostatic repulsion arising from their hydrated molecular dimension and the negative surface charge of the membranes. On the other hand, there was no

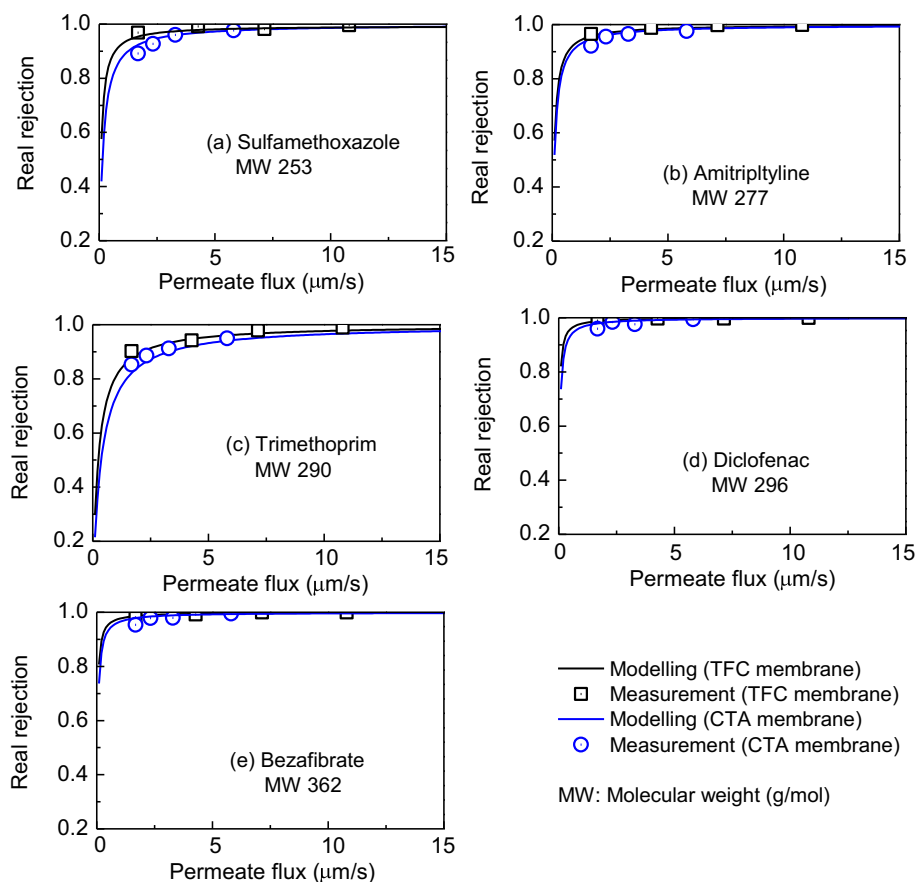


**Fig. 3** – Real rejection of the charged trace organic contaminants as a function of permeate water flux by the CTA and TFC membranes. The symbols represent experimental data for the specific trace organic contaminant, while the solid lines represent the membrane pore hindrance transport model predictions with the optimized parameters listed in Table 3. Other conditions are as detailed in Fig. 2.

discernible difference in the rejection of charged TrOCs by the two membranes. Further, the TFC membrane exhibited substantially higher rejection of neutral TrOCs than the CTA membrane, despite its larger membrane pore size (Table 3). This observation was consistent with our hypothesis proposed in Section 3.1.3 that the hydrated membrane pore surface induced by the existence of surface charge narrowed the effective membrane pore size, thereby enhancing the steric hindrance and resulting in better separation performance. This hypothesis will be further elaborated using the membrane pore hindrance transport model for a wide range of permeate water flux values in the following section.

### 3.2.2. Modelling the rejection of trace organic contaminants

The calculated membrane pore radii (Table 3) and the molecular radius of each compound can be used to simulate the

rejection of TrOCs as a function of permeate water flux based on the membrane pore hindrance transport model (see Section 2.3.2). This model was found to describe very well the real rejection of TrOCs by both the CTA and TFC membranes. Overall, the real rejection of TrOCs by both membranes increased as permeate flux increased, consistent with the phenomenon observed in pressure driven NF and RO processes (Nghiem et al., 2004).

Real rejections of charged TrOCs were above 90% for both CTA and TFC membranes (Fig. 3). For negatively charged TrOCs, electrostatic repulsion arising from the negative surface charge of the membranes played an important role in their rejection. For example, despite similar molecular weight of sulfamethoxazole and linuron, real rejection of the negatively charged sulfamethoxazole (0.90 by the CTA membrane and 0.98 by the TFC membrane) was substantially higher than

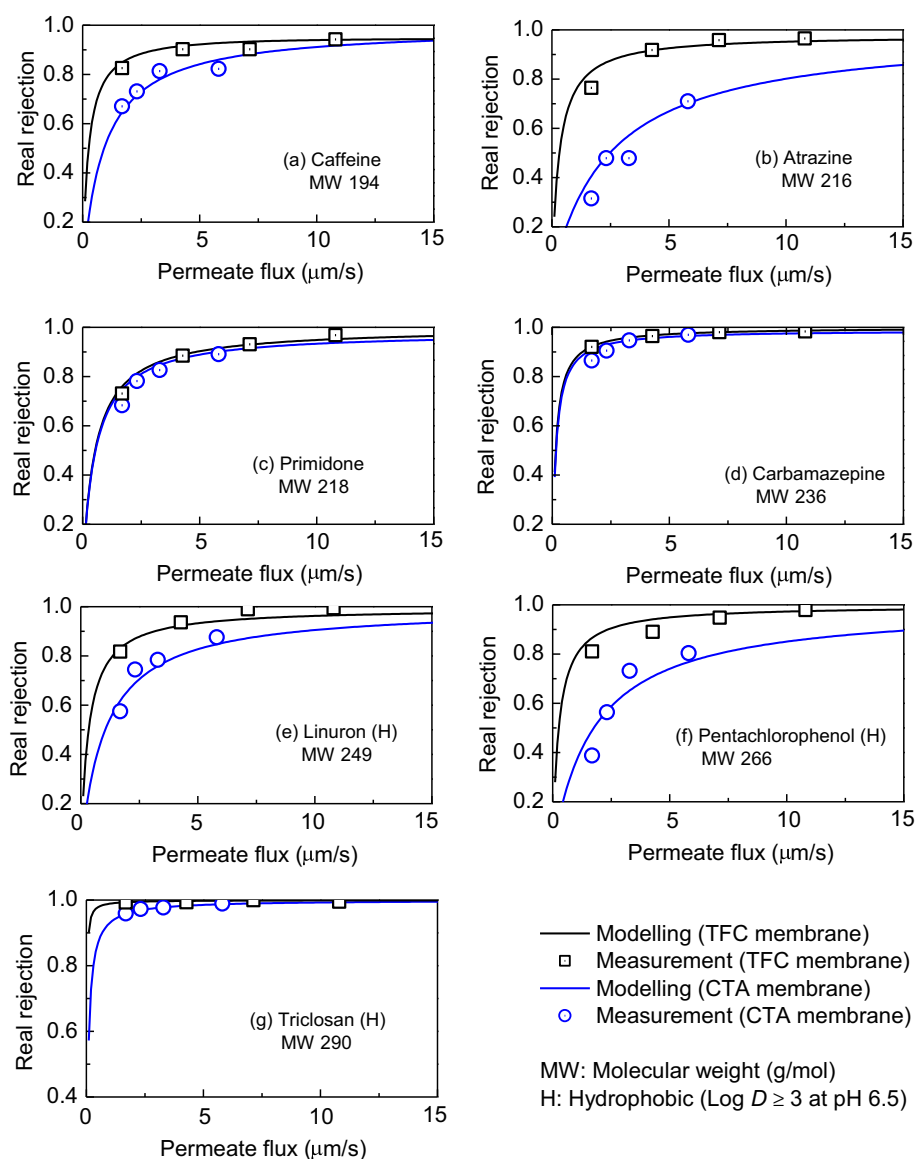


**Fig. 4 – Real rejection of the neutral trace organic contaminants as a function of permeate water flux by the CTA and TFC membranes. The symbols represent experimental data for the specific trace organic contaminant, while the solid lines represent the membrane pore hindrance transport model predictions with the optimized parameters listed in Table 2. Other conditions are as described in Fig. 2.**

the neutral linuron (0.59 by the CTA membrane and 0.82 by the TFC membrane). More significantly, there was marginal difference in real rejection of negatively charged TrOCs as their molecular weight increased. In aqueous solution, the charged TrOCs are hydrated and their hydrated radii are significantly larger than their apparent ionic radii (Nghiem et al., 2006). As a result, steric hindrance also governs the separation of both negatively and positively charged TrOCs. In summary, both electrostatic repulsion and steric hindrance govern the rejection of charged TrOCs in FO, thereby resulting in their high rejection.

Generally, the TFC membrane exhibited higher rejection of hydrophilic neutral (caffeine and atrazine) and hydrophobic neutral (linuron and pentachlorophenol) TrOCs with low molecular weights (Fig. 4). As the molecular weight increased, there was no discernible difference in the rejection of neutral hydrophilic and hydrophobic TrOCs by either the CTA or TFC membranes. This molecular-weight dependent rejection behaviour suggests that steric hindrance governs the rejection of neutral TrOCs in an FO process. However, it is noteworthy that despite its larger effective pore size compared to that of the CTA membrane, the TFC membrane exhibited higher rejection of neutral TrOCs with low molecular weight than the CTA membrane.

**3.2.3. Relating trace organic rejection to membrane properties**  
Structure of the membrane active layer plays an important role in the rejection of TrOCs. Active layer structures of the CTA and TFC membranes differed significantly. The TFC membrane has a higher  $l/\epsilon$  parameter and thus exhibits higher hindrance to TrOC diffusion in comparison to the CTA membrane. The higher solute hindrance of the TFC membrane is also consistent with its lower  $B$  value, which can be described by the “solution–diffusion” mechanism in the FO process (Hancock et al., 2011a; Yong et al., 2012).

Pore hydration induced by membrane surface charge also attributed to the higher TrOC rejection by the TFC membrane. Pore hydration exists in both the CTA and TFC membranes, which is manifested by a layer of water molecules permanently attached to the negatively charged membrane surface via hydrogen bonding (Raghunathan and Aluru, 2006). However, the degrees of pore hydration of the CTA and TFC membranes were likely different when they are operated in FO mode because of the difference in reverse NaCl permeation (Fig. 5). Specifically, the CTA membrane possessed less surface charge (Fig. 1) and exhibited an order of magnitude higher reverse NaCl flux than the TFC membrane (Table 4). Thus, pore hydration of the CTA membrane was substantially suppressed due to the elevated ionic strength in the membrane pore (Nghiem et al., 2006). By contrast, the TFC membrane has a much lower reverse NaCl salt flux due to a more negative membrane surface charge in comparison to the CTA membrane. Thus, TFC membrane pores remain highly hydrated in FO mode, resulting in a higher TrOC rejection when compared to the CTA membrane.

Results reported here have significant implications for the fabrication of next generation FO membranes. The separation performance of FO membranes could be improved substantially by tuning both the active layer structure and surface charge. Fabricating an active layer with superior transport properties is important in achieving better TrOC rejections (Tiraferri et al., 2011), such as high  $A$  and low  $B$  values, and high  $l/\epsilon$  value. Imparting surface charge to the membrane could offer enhanced steric hindrance without compromising water diffusion. In a recent study, Flanagan and Escobar (2013) modified a neutral polybenzimidazole based membrane using different functional agents to impart negative surface charges and reported higher water flux and NaCl rejection than unmodified PBI membrane. However, the possible detrimental effects of carboxyl groups on the membrane resistance to organic fouling should be

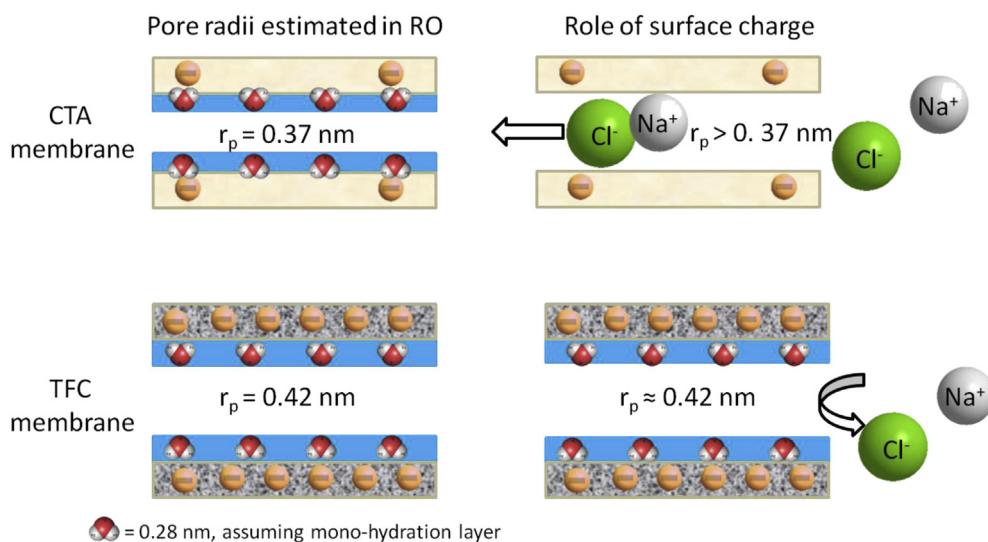


**Fig. 5 – A conceptual illustration of the role of surface charge in enhancing solute rejection in an FO process. The estimated membrane pore radii and hydration layers of the CTA and TFC membranes are illustrated on left-hand column; the role of surface charge and hydration of membrane pores in FO are shown on right-hand column.**



considered (Mo et al., 2012), which requires optimization of charge density and type of functional groups.

#### 4. Conclusions

We have systematically characterised key properties of the CTA and TFC membranes and compared their rejection of 12 TrOCs as a function of permeate flux using the membrane pore hindrance transport model. The TFC membrane has a higher A value, lower B and S values and higher surface charge than those of the CTA membrane. As a result, the TFC membrane exhibited a higher water flux and lower reverse NaCl flux than the CTA membrane. More importantly, the calculated membrane pore radii of the CTA and TFC membranes were 0.37 and 0.42 nm, respectively. The calculated active layer structure factor,  $l/\epsilon$ , of the CTA and TFC membranes were 0.11 and 2.12  $\mu\text{m}$ , respectively.

The pore hindrance transport model can be used to describe the rejection of TrOCs by the FO process. Rejection of charged TrOCs by both the CTA and TFC membranes was generally high and was governed by both electrostatic interaction and steric hindrance. In contrast, the TFC membrane exhibited higher rejection of neutral TrOCs with low molecular weight than the CTA membrane, albeit that the TFC membrane pore size was larger than that for the CTA membrane. We attribute the observed higher rejection of neutral TrOCs by the TFC membrane to a more favourable active layer structure as indicated by the larger active layer thickness to porosity ratio parameter,  $l/\epsilon$ , and the negative membrane surface charge that induced pore hydration.

#### Acknowledgements

This study was supported by the Australian Research Council Discovery Project DP140103864. The authors would like to thank Hydration Technology Innovations and Oasys Water for providing membrane samples. University of Wollongong is acknowledged for the provision of a doctoral scholarship to Ming Xie.

#### REFERENCES

- Alturki, A.A., McDonald, J.A., Khan, S.J., Price, W.E., Nghiem, L.D., Elimelech, M., 2013. Removal of trace organic contaminants by the forward osmosis process. *Sep. Purif. Technol.* 103, 258–266.
- Basile, T., Petrella, A., Petrella, M., Boghetich, G., Petruzzelli, V., Colasuonno, S., Petruzzelli, D., 2011. Review of endocrine-disrupting-compound removal technologies in water and wastewater treatment plants: an EU perspective. *Ind. Eng. Chem. Res.* 50 (14), 8389–8401.
- Bungay, P.M., Brenner, H., 1973. The motion of a closely-fitting sphere in a fluid-filled tube. *Int. J. Multiphase Flow* 1 (1), 25–56.
- Carballa, M., Omil, F., Lema, J.M., Llompарт, M.a., Garcia-Jares, C., Rodriguez, I., Gómez, M., Ternes, T., 2004. Behavior of pharmaceuticals, cosmetics and hormones in a sewage treatment plant. *Water Res.* 38 (12), 2918–2926.
- Cartinella, J.L., Cath, T.Y., Flynn, M.T., Miller, G.C., Hunter, K.W., Childress, A.E., 2006. Removal of natural steroid hormones from wastewater using membrane contactor processes†. *Environ. Sci. Technol.* 40 (23), 7381–7386.
- Cath, T.Y., Adams, D., Childress, A.E., 2005. Membrane contactor processes for wastewater reclamation in space: II. Combined direct osmosis, osmotic distillation, and membrane distillation for treatment of metabolic wastewater. *J. Memb. Sci.* 257 (1–2), 111–119.
- Cath, T.Y., Childress, A.E., Elimelech, M., 2006. Forward osmosis: principles, applications, and recent developments. *J. Memb. Sci.* 281 (1–2), 70–87.
- Cath, T.Y., Elimelech, M., McCutcheon, J.R., McGinnis, R.L., Achilli, A., Anastasio, D., Brady, A.R., Childress, A.E., Farr, I.V., Hancock, N.T., Lampi, J., Nghiem, L.D., Xie, M., Yip, N.Y., 2013. Standard methodology for evaluating membrane performance in osmotically driven membrane processes. *Desalination* 312, 31–38.
- Cath, T.Y., Hancock, N.T., Lundin, C.D., Hoppe-Jones, C., Drewes, J.E., 2010. A multi-barrier osmotic dilution process for simultaneous desalination and purification of impaired water. *J. Memb. Sci.* 362 (1–2), 417–426.
- Childress, A.E., Elimelech, M., 1996. Effect of solution chemistry on the surface charge of polymeric reverse osmosis and nanofiltration membranes. *J. Memb. Sci.* 119 (2), 253–268.
- Elimelech, M., Chen, W.H., Waypa, J.J., 1994. Measuring the zeta (electrokinetic) potential of reverse osmosis membranes by a streaming potential analyzer. *Desalination* 95 (3), 269–286.
- Elimelech, M., O'Melia, C.R., 1990. Effect of electrolyte type on the electrophoretic mobility of polystyrene latex colloids. *Colloid. Surf.* 44, 165–178.
- Elimelech, M., Phillip, W.A., 2011. The future of seawater desalination: energy, technology, and the environment. *Science* 333 (6043), 712–717.
- Flanagan, M.F., Escobar, I.C., 2013. Novel charged and hydrophilized polybenzimidazole (PBI) membranes for forward osmosis. *J. Memb. Sci.* 434, 85–92.
- Grant, S.B., Saphores, J.-D., Feldman, D.L., Hamilton, A.J., Fletcher, T.D., Cook, P.L.M., Stewardson, M., Sanders, B.F., Levin, L.A., Ambrose, R.F., Deletic, A., Brown, R., Jiang, S.C., Rosso, D., Cooper, W.J., Marusic, I., 2012. Taking the “Waste” out of “Wastewater” for human water security and ecosystem sustainability. *Science* 337 (6095), 681–686.
- Hancock, N.T., Phillip, W.A., Elimelech, M., Cath, T.Y., 2011a. Bidirectional permeation of electrolytes in osmotically driven membrane processes. *Environ. Sci. Technol.* 45 (24), 10642–10651.
- Hancock, N.T., Xu, P., Heil, D.M., Bellona, C., Cath, T.Y., 2011b. Comprehensive bench- and pilot-scale investigation of trace organic compounds rejection by forward osmosis. *Environ. Sci. Technol.* 45 (19), 8483–8490.
- Hoover, L.A., Phillip, W.A., Tiraferri, A., Yip, N.Y., Elimelech, M., 2011. Forward with osmosis: emerging applications for greater sustainability. *Environ. Sci. Technol.* 45 (23), 9824–9830.
- Martinetti, C.R., Childress, A.E., Cath, T.Y., 2009. High recovery of concentrated RO brines using forward osmosis and membrane distillation. *J. Memb. Sci.* 331 (1–2), 31–39.
- McCutcheon, J.R., Elimelech, M., 2008. Influence of membrane support layer hydrophobicity on water flux in osmotically driven membrane processes. *J. Memb. Sci.* 318 (1–2), 458–466.
- McCutcheon, J.R., McGinnis, R.L., Elimelech, M., 2005. A novel ammonia–carbon dioxide forward (direct) osmosis desalination process. *Desalination* 174 (1), 1–11.
- McGinnis, R.L., Elimelech, M., 2007. Energy requirements of ammonia–carbon dioxide forward osmosis desalination. *Desalination* 207 (1–3), 370–382.
- McGinnis, R.L., Hancock, N.T., Nowosielski-Slepowron, M.S., McGurgan, G.D., 2013. Pilot demonstration of the  $\text{NH}_3/\text{CO}_2$

- forward osmosis desalination process on high salinity brines. *Desalination* 312, 67–74.
- Mi, B., Elimelech, M., 2010. Gypsum scaling and cleaning in forward osmosis: measurements and mechanisms. *Environ. Sci. Technol.* 44 (6), 2022–2028.
- Mo, Y., Tiraferri, A., Yip, N.Y., Adout, A., Huang, X., Elimelech, M., 2012. Improved antifouling properties of polyamide nanofiltration membranes by reducing the density of surface carboxyl groups. *Environ. Sci. Technol.* 46 (24), 13253–13261.
- Nghiem, L.D., Schafer, A.I., Elimelech, M., 2006. Role of electrostatic interactions in the retention of pharmaceutically active contaminants by a loose nanofiltration membrane. *J. Memb. Sci.* 286 (1–2), 52–59.
- Nghiem, L.D., Schäfer, A.I., Elimelech, M., 2004. Removal of natural hormones by nanofiltration membranes: measurement, modeling, and mechanisms. *Environ. Sci. Technol.* 38 (6), 1888–1896.
- Petersen, R.J., 1993. Composite reverse osmosis and nanofiltration membranes. *J. Memb. Sci.* 83 (1), 81–150.
- Raghunathan, A.V., Aluru, N.R., 2006. Molecular understanding of osmosis in semipermeable membranes. *Phys. Rev. Lett.* 97 (2), 024501.
- Schäfer, A.I., Akanyeti, I., Semião, A.J.C., 2011. Micropollutant sorption to membrane polymers: a review of mechanisms for estrogens. *Adv. Colloid Interface Sci.* 164 (1–2), 100–117.
- Schwarzenbach, R.P., Escher, B.I., Fenner, K., Hofstetter, T.B., Johnson, C.A., von Gunten, U., Wehrli, B., 2006. The challenge of micropollutants in aquatic systems. *Science* 313 (5790), 1072–1077.
- Shaffer, D.L., Yip, N.Y., Gilron, J., Elimelech, M., 2012. Seawater desalination for agriculture by integrated forward and reverse osmosis: improved product water quality for potentially less energy. *J. Memb. Sci.* 415–416, 1–8.
- Shannon, M.A., Bohn, P.W., Elimelech, M., Georgiadis, J.G., Marinas, B.J., Mayes, A.M., 2008. Science and technology for water purification in the coming decades. *Nature* 452 (7185), 301–310.
- Snyder, S.A., Westerhoff, P., Yoon, Y., Sedlak, D.L., 2003. Pharmaceuticals, personal care products, and endocrine disruptors in water: implications for the water industry. *Environ. Eng. Sci.* 20 (5), 449–469.
- Sutzkover, I., Hasson, D., Semiat, R., 2000. Simple technique for measuring the concentration polarization level in a reverse osmosis system. *Desalination* 131 (1–3), 117–127.
- Tiraferri, A., Elimelech, M., 2012. Direct quantification of negatively charged functional groups on membrane surfaces. *J. Memb. Sci.* 389, 499–508.
- Tiraferri, A., Yip, N.Y., Phillip, W.A., Schiffman, J.D., Elimelech, M., 2011. Relating performance of thin-film composite forward osmosis membranes to support layer formation and structure. *J. Memb. Sci.* 367 (1–2), 340–352.
- Valladares Linares, R., Yangali-Quintanilla, V., Li, Z., Amy, G., 2011. Rejection of micropollutants by clean and fouled forward osmosis membrane. *Water Res.* 45 (20), 6737–6744.
- Wang, R., Shi, L., Tang, C.Y., Chou, S., Qiu, C., Fane, A.G., 2010. Characterization of novel forward osmosis hollow fiber membranes. *J. Memb. Sci.* 355 (1–2), 158–167.
- Wei, J., Qiu, C., Tang, C.Y., Wang, R., Fane, A.G., 2011. Synthesis and characterization of flat-sheet thin film composite forward osmosis membranes. *J. Memb. Sci.* 372 (1–2), 292–302.
- Wilke, C.R., Chang, P., 1955. Correlation of diffusion coefficients in dilute solutions. *AIChE J.* 1 (2), 264–270.
- Xie, M., Nghiem, L.D., Price, W.E., Elimelech, M., 2012a. Comparison of the removal of hydrophobic trace organic contaminants by forward osmosis and reverse osmosis. *Water Res.* 46 (8), 2683–2692.
- Xie, M., Price, W.E., Nghiem, L.D., 2012b. Rejection of pharmaceutically active compounds by forward osmosis: role of solution pH and membrane orientation. *Sep. Puri. Technol.* 93, 107–114.
- Xie, M., Price, W.E., Nghiem, L.D., Elimelech, M., 2013. Effects of feed and draw solution temperature and transmembrane temperature difference on the rejection of trace organic contaminants by forward osmosis. *J. Memb. Sci.* 438, 57–64.
- Yangali-Quintanilla, V., Li, Z., Valladares, R., Li, Q., Amy, G., 2011. Indirect desalination of Red Sea water with forward osmosis and low pressure reverse osmosis for water reuse. *Desalination* 280 (1–3), 160–166.
- Yip, N.Y., Tiraferri, A., Phillip, W.A., Schiffman, J.D., Elimelech, M., 2010. High performance thin-film composite forward osmosis membrane. *Environ. Sci. Technol.* 44 (10), 3812–3818.
- Yong, J.S., Phillip, W.A., Elimelech, M., 2012. Coupled reverse draw solute permeation and water flux in forward osmosis with neutral draw solutes. *J. Memb. Sci.* 392–393, 9–17.
- Zhao, S., Zou, L., Tang, C.Y., Mulcahy, D., 2012. Recent developments in forward osmosis: opportunities and challenges. *J. Memb. Sci.* 396, 1–21.